analytical chemistry

pubs.acs.org/ac Article

Versatile Sensing Platform for Cd^{2+} Detection in Rice Samples and Its Applications in Logic Gate Computation

Junhua Chen,* Jiafeng Pan, and Chengshuai Liu

Cite This: *Anal. Chem.* 2020, 92, 6173−6180 Read Online

ACCESS | Metrics & More | Article Recommendations | Supporting Information

ABSTRACT: A versatile sensing platform was designed for Cd^{2+} detection utilizing Mg^{2+}-dependent DNAzyme as the biocatalyst and toehold-mediated strand replacement as the reaction mechanism. The Cd^{2+}−aptamer interaction brings the split subunits of the Mg^{2+}-dependent DNAzyme into close-enough proximity, which generates an active DNAzyme that can catalyze the cleavage reaction toward the hairpin substrate strand (H1). The trigger DNA fragment in H1 can open another hairpin probe (H2) to activate the cyclic signal amplification process. The generated numerous G-quadruplex DNAzyme structures will produce a high fluorescence response after incubation with the fluorescence dye *N*-methyl mesoporphyrin IX (NMM). This detection platform is ultrasensitive and the detection limit (LOD) is 2.5 pM (S/N = 3). The sensing system is robust and can work effectively even in a complex sample matrix, enabling the quantitative analysis of Cd^{2+} content in rice samples with good reliability. Showing the unique features of simple operation, label-free and enzyme-free format, high sensitivity and selectivity, and universal signal amplification mode, our proposed sensing protocol holds great promise for becoming a competitive alternative for the routine monitoring of Cd^{2+} pollution. Importantly, this flexible and versatile sensing platform was used to construct some exquisite logic gates, including AND, OR, INHIBIT, IMPLICATION, NOR, and NAND.

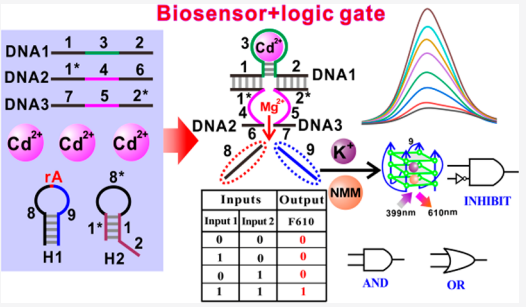

As a typical heavy metal pollutant, cadmium ions (Cd^{2+}) are detrimental to the ecosystem, food safety, and human health.[1] The excess content of Cd^{2+} is highly toxic and can cause serious diseases.[2] Considering its ubiquity and toxicity, the maximum allowable concentration of Cd^{2+} in drinking water was set to be 5 ppb by the U.S. Environmental Protection Agency (EPA).[3] Traditional methods for Cd^{2+} detection focused on atomic absorption/fluorescence spectrometry[4,5] and inductively coupled plasma-mass spectrometry (ICP-MS).[6] Although they are precise, complex sample pretreatment, skilled technicians, and expensive instrument are required,[7] which limits their wide applications for routine testing. Thus, there is still a great demand to design fast, low cost, and reliable detection methods for Cd^{2+} analysis in real samples.

To construct sensors for Cd^{2+} detection, molecular recognition probes have proven to be indispensable for Cd^{2+} binding.[8] In recent years, some exquisite detection methods have been reported using antibodies,[9,10] chelators,[11−14] DNAzymes,[15,16] and aptamers[17−20] as the binding ligands for Cd^{2+} detection. Among them, aptamer possesses the remarkable advancement in biosensor design, such as high stability and reversible denaturation, easy chemical synthesis and modification, and controllable and predictable conformation changes after target binding.[21] In this work, the anti-Cd^{2+} aptamer[22−24] was employed as the binding sequence to fabricate the Cd^{2+} biosensor.

For heavy metal ion detection, high sensitivity is often desirable.[25] Thus, signal amplification strategy is often integrated into the biosensor architecture.[26] Protein-based enzymes are commonly used to receive signal amplification, such as exonuclease,[27,28] nicking enzyme,[29,30] and polymerase.[31,32] Enzyme-free signal amplification strategies were also utilized to construct sensitive biosensors, most of which originated from the toehold-mediated DNA strand displacement.[33] Recently, metal ion-dependent DNAzyme appeared as an ideal amplifier to receive improved detection signals.[34] For example, the Mg^{2+}-dependent DNAzyme can catalyze the cleavage reaction toward the substrate strand and offer continuous signal conversion capability.[35] Thus, each aptamer binding event or target recognition reaction can be converted into numerous signal generating probes.[36] With the attractive characteristics of multiple catalytic activities, high stability, and enzyme-free format,[37,38] Mg^{2+}-dependent DNAzyme was used in this study as the biocatalyst to amplify the response signals.

Molecular logic gates with multiple biocomputing capabilities can be used to construct a smart sensing system for

Received: March 7, 2020
Accepted: March 25, 2020
Published: March 25, 2020

https://dx.doi.org/10.1021/acs.analchem.0c01022
Anal. Chem. 2020, 92, 6173−6180

intelligent detection and disease diagnostics.[39] In the logic binary operation, 1 and 0 were used to encode the inputs, with the presence and absence of the target assigned as 1 and 0, respectively. For output, 1 was used to indicate a high signal, while 0 was used to show a low signal.[40] The decision-making capability endows logic gate as a powerful tool in the rapid screening of multiple pollutants in the environmental and food samples.[41] In this work, we further extend our versatile sensing system to the fabrication of some interesting logic gates, such as AND, OR, INHIBIT, IMPLICATION, NOR, and NAND. To demonstrate the robustness of the logic gate, we employed the OR logic gate to be operated in rice samples. The results indicated that our constructed logic system can perform the logic functions well even in complex sample matrixes, suggesting the great potential of the logic gates for the intelligent detection of heavy metal ions in real samples.

EXPERIMENTAL SECTION

Reagents and Materials. *N*-Methyl mesoporphyrin IX (NMM) and Tris were purchased from Sigma-Aldrich (St. Louis, MO). Other chemicals were of analytical grade. The buffer was prepared using Milli-Q water (18.2 MΩ/cm). The HPLC-purified oligonucleotides were ordered from Sangon Biotech. Co. Ltd. (Shanghai, China), and their sequences were listed in Table S1 (Supporting Information).

Analytical Procedure for Cd^{2+} Detection. All of the nucleic acid probes were dissolved into 50 mM Tris-HCl buffer solution (pH 7.4, 150 mM NaCl, 100 mM KCl, and 50 mM $MgCl_2$). 100 nM DNA1 was incubated with different concentrations of Cd^{2+} for 40 min. Then, 200 nM DNA2 and 200 nM DNA3 were added and incubated for 30 min. Subsequently, 250 nM H1 and 300 nM H2 were introduced into the above solution and incubated for 120 min. Finally, 1.5 μM NMM was added and incubated at room temperature for 15 min. The fluorescence spectra were recorded from 550 to 680 nm (E_x = 399 nm, E_m = 610 nm). The fluorescence measurements were carried out on the SpectraMax i3x (Molecular Devices).

To investigate the selectivity of this biosensor, other metal ions, including Ag^+, Cu^{2+}, Fe^{2+}, Mn^{2+}, Ni^{2+}, Ca^{2+}, As^{3+}, Al^{3+}, As^{5+}, Hg^{2+}, Pb^{2+}, and Cr^{3+} at 100 nM were tested in the same way.

Cd^{2+} Detection in Rice Samples. Contaminated rice samples were triturated by a blender. A total of 1 g of the rice powder was mixed with HNO_3 (7 mL) and 30% H_2O_2 (3 mL). After incubation at 95 °C for 3 h, the mixture was then cooled to room temperature. After digestion, the cadmium was almost converted into divalent cadmium (Cd^{2+}),[42,43] which is stable in nature. Particulates in the digestion were removed by filtration. The solution is diluted to 50-fold, and the pH of the aqueous rice sample was adjusted to 7. The concentration of Cd^{2+} in rice samples was detected using our proposed biosensor. Also, the ICP-MS assay was employed to verify the biosensor results.

Procedures for Logic Gate Operation. In the AND logic gate operation, 100 nM Cd^{2+} and 100 nM DNA1 were used as the two inputs to activate the sensing platform. Other procedures were the same as that for Cd^{2+} detection in the sensing system.

In the OR logic gate operation, 100 nM Cd^{2+} and 50 nM DNA4 were used as the two inputs to activate the sensing platform. Other procedures were the same as that for Cd^{2+} detection in the sensing system.

In the INBIHIT logic gate operation, 100 nM Cd^{2+} was hybridized with 100 nM DNA1 to form the Cd^{2+}−DNA1 complex, which was used as the input 1. DNA5 (100 nM) was used as the input 2. Other procedures were the same as that for Cd^{2+} detection in the sensing system.

In the IMPLICATION logic gate operation, 100 nM Cd^{2+} was hybridized with 100 nM DNA6 to form the Cd^{2+}−DNA6 complex, which was used as the input 1. DNA7 (100 nM) was used as the input 2. DNA8 (50 nM) was also used as the sensing component. Other procedures were the same as that for Cd^{2+} detection in the sensing system.

In the NOR logic gate operation, 100 nM Cd^{2+} was hybridized with 100 nM DNA6 to form the Cd^{2+}−DNA6 complex, which was used as the input 1. DNA9 (100 nM) was used as the input 2. DNA10 (50 nM) was also used as the sensing component. Other procedures were the same as that for Cd^{2+} detection in the sensing system.

In the NAND logic gate operation, 100 nM Cd^{2+} was hybridized with 100 nM DNA6 to form the Cd^{2+}−DNA6 complex, which was used as the input 1. DNA9 (100 nM) was used as the input 2. DNA11 (50 nM) was also used as the sensing component. Other procedures were the same as that for Cd^{2+} detection in the sensing system.

Native Polyacrylamide Gel Electrophoresis (PAGE). The DNA samples were mixed with 6× loading buffer and analyzed in 15% native polyacrylamide gel. The electrophoresis experiment was carried out in 1× TBE buffer (pH 8.0). All gels were run for 90 min at 100 V at room temperature. After running, the gels were stained for 25 min with 1× SYBR Green solution. All gels were imaged with a Gel Doc XR+ system (Bio-Rad).

Circular Dichroism (CD) Spectroscopy. CD spectra were measured on a Chirascan circular dichroism spectrometer (Applied Photophysics Ltd., England, U.K.) at room temperature. The DNA was prepared in 50 mM Tris-Ac buffer solution (pH 7.4, 150 mM NaAc, 100 mM KAc, and 50 mM $Mg(Ac)_2$). The CD spectra were obtained from 220 to 330 nm in 1 mm path length cuvettes and averaged from three scans with the buffer background subtracted.

RESULTS AND DISCUSSION

Sensing Principle for Cd^{2+} Detection. The sensing principle of our proposed sensing strategy for Cd^{2+} detection is schematically illustrated in Figure 1. Domain 3 of DNA1 is the Cd^{2+}-specific aptamer sequence, which can bind with Cd^{2+} with high affinity. Domain 4 of DNA2 and domain 5 of DNA3 are the split subunits of the Mg^{2+}-dependent DNAzyme. The DNA sequences were listed in Table S1 (Supporting Information). In the presence of Cd^{2+}, the interaction between Cd^{2+} and DNA1 brings domains 1 and 2 into close-enough proximity, which can hybridize with the domain 1* of DNA2 and the domain 2* of DNA3, respectively. The synergistically stabilized DNA structure (DNA1−DNA2−DNA3) generates an active Mg^{2+}-dependent DNAzyme. As the domains 6 and 7 are complementary to the loop section of the substrate strand (H1), in the presence of Mg^{2+}, H1 will be cleaved into two fragments (domains 8 and 9). Domain 9 contains the G-rich sequence, which can fold into the G-quadruplex structure in the presence of *N*-methyl mesoporphyrin IX (NMM) and K^+. NMM can bind to the G-quadruplex structure with high selectivity, but it cannot bind to the duplex or single-stranded DNA.[44] The free NMM exhibits a weak fluorescence response. Upon binding to the G-quadruplex DNA, the fluorescence

https://dx.doi.org/10.1021/acs.analchem.0c01022
Anal. Chem. 2020, 92, 6173−6180

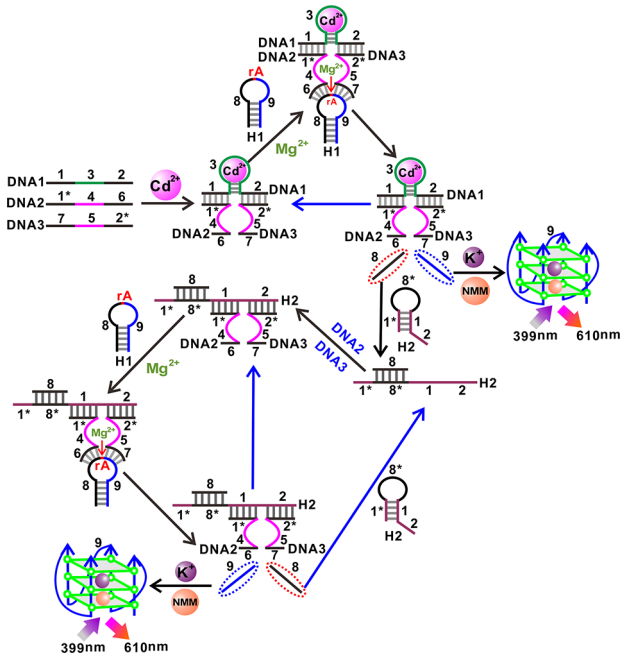

Figure 1. Schematic illustration of the detection mechanism for Cd^{2+} based on DNAzyme-mediated cyclic signal amplification strategy. Domain 3 of DNA1 is the Cd^{2+}-specific aptamer sequence. Domain 4 of DNA2 and domain 5 of DNA3 are the split subunits of the Mg^{2+}-dependent DNAzyme.

intensity of NMM can be improved sharply.[45] At the same time, another liberated fragment (domain 8) is the trigger DNA, which will initiate the cyclic assembly of other active DNAzymes for signal amplification.

Domain 8 then hybridizes with domains 8* of H2, opening the hairpin H2 to expose domains 1 and 2. The synergistic hybridization among the opened H2, DNA2, and DNA3 forms another active Mg^{2+}-dependent DNAzyme that can also bind to H1. The cleavage reaction toward H1 results in the release of the blocked G-rich DNA (domain 9) and the occluded trigger DNA (domain 8). After hybridization with H2, domain 8 will enter into another cyclic assembly process, resulting in the generation of numerous free G-rich sequences. Importantly, each activated Mg^{2+}-dependent DNAzyme possesses multiple signal conversion capabilities, which can catalyze the continuous cleavage of H1 substrates, thus generating an amplified signal for Cd^{2+} detection. In the absence of Cd^{2+}, domain 1 and domain 2 in DNA1 are kept separated, which inhibited the formation of active Mg^{2+}-dependent DNAzyme. The cleavage reaction to H1 cannot happen and the caged G-rich DNA (domain 9) is still blocked in H1. Thus, without the target Cd^{2+} in the sensing system, only weak fluorescence signal can be observed.

Feasibility Assay. The feasibility of the signal amplification strategy for Cd^{2+} sensing was verified by testing the solution at different controls. As shown in Figure S1 (Supporting Information), only a weak background signal can be observed in the absence of Cd^{2+} (curve a). This indicated that without target Cd^{2+}, no active Mg^{2+}-dependent DNAzyme can be formed and the G-rich DNA was still in a caged state. In the presence of Cd^{2+} but without H2, a remarkable signal can be observed (curve b). This increase of fluorescence intensity can be attributed to the formation of an active Mg^{2+}-dependent DNAzyme, which can catalyze the cleavage reaction to H1 and liberate the caged G-rich sequence. When H2 was also present in the sensing system, the response signal was sharply increased (curve c). The reason is that the released domain 8 after the cleavage reaction can open H2 to trigger the cyclic signal amplification process. Thus, numerous H1 substrates will be cleaved into two fragments and lots of G-quadruplex can be generated to give an amplified signal for the target Cd^{2+} detection. Meanwhile, the corresponding fluorescence colors were recorded in the dark to confirm the feasibility of the sensor (inset in Figure S1). The reaction process of the sensing system was further confirmed by the PAGE images (Figure S2A, Supporting Information). The formation of the G-quadruplex structure was also verified by the CD results (Figure S2B, Supporting Information).

Analytical Performance. Under the optimal assay conditions (Figures S3–S6, Supporting Information), we investigate the linear range and detection limit of the biosensor for Cd^{2+} detection. As shown in Figure 2A, a gradual increase

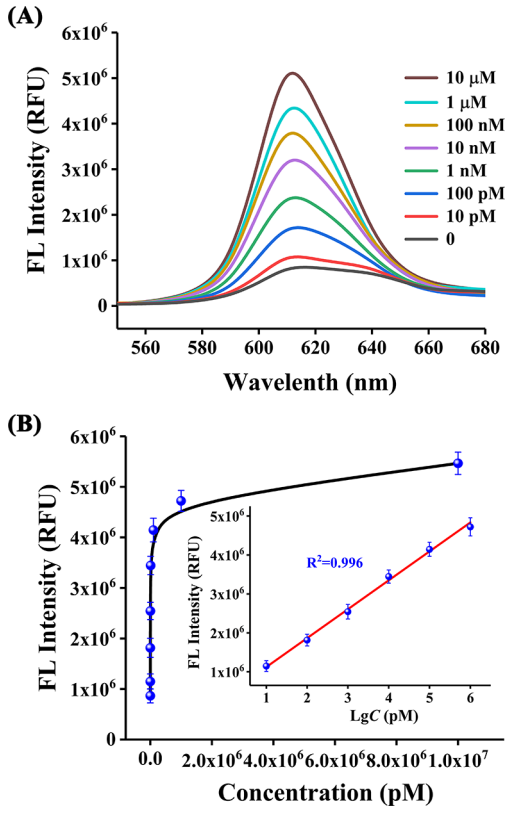

Figure 2. (A) Fluorescence responses of the solution containing different concentrations of Cd^{2+}. (B) Plots of the fluorescence value at 610 nm as a function of the Cd^{2+} concentration. Inset: The linear range analysis of the Cd^{2+} biosensor.

of the fluorescence signal was achieved as the Cd^{2+} concentration increased from 0 to 10 μM. The fluorescence values at 610 nm were recorded in Figure 2B. The corresponding calibration curve shows that the fluorescence intensity is proportional to the logarithm of Cd^{2+} concentration ranging from 10 pM to 1 μM (inset of Figure 2B). The linear regression equation was set as $F = 7.43 \times 10^5 \lg C + 3.8 \times 10^5$ ($R^2 = 0.996$) (F, fluorescence value at 610 nm; C, Cd^{2+} concentration). The LOD is calculated to be 2.5 pM based on 3S/N. This LOD of the proposed sensing system is comparable or even superior to some previously reported

https://dx.doi.org/10.1021/acs.analchem.0c01022
Anal. Chem. 2020, 92, 6173−6180

Cd^{2+} methods (Table S2, Supporting Information). Such excellent sensitivity can ascribe to the continuous signal amplification and multiple signal conversion capability by Mg^{2+}-dependent DNAzyme.

Selectivity of the Sensor. To examine the selectivity of the constructed biosensor for Cd^{2+} detection, several other control heavy metal ions, such as Ag^{+}, Cu^{2+}, Fe^{2+}, Mn^{2+}, Ni^{2+}, Ca^{2+}, As^{3+}, Al^{3+}, As^{5+}, Hg^{2+}, Pb^{2+}, and Cr^{3+} were also tested in the same way. As shown in Figure 3, 1 nM Cd^{2+} can result in a significant increase of the fluorescence intensity. Other metal ions even with the concentrations of 100 nM failed to generate obvious fluorescence changes in the sensing system. The above data demonstrated that this sensing platform possessed excellent specificity for the Cd^{2+} assay. The control heavy metal ions did not disturb the biosensor response. This high specificity can be ascribed to the high binding capability between Cd^{2+} and the aptamer.

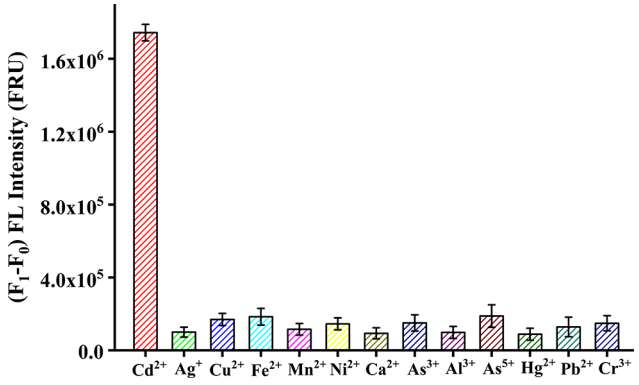

Figure 3. Selectivity testing of the sensing system for Cd^{2+} and some control metal ions. F_1 is the fluorescence value of the solution with 1 nM Cd^{2+} or 100 nM other metal ions. F_0 is the fluorescence value of the blank solution. The Ag^{+} was tested in 50 mM Tris-Ac buffer solution (pH 7.4, 150 mM NaAc, 100 mM KAc, and 50 mM $Mg(Ac)_2$).

Real Sample Analysis. To demonstrate the practical applications of the sensing platform, this biosensor was applied to the detection of Cd^{2+} in rice samples. The Cd^{2+} content in different rice samples were verified using the ICP-MS method. The analysis results are listed in Table S3 (Supporting Information). The data revealed that no significant difference existed between the present biosensor and the ICP-MS method. Such good accuracy and satisfactory reliability enable the biosensor to be developed as an ideal detection tool for Cd^{2+} monitoring in real samples.

AND Logic Gate. Our constructed sensing system is flexible and versatile, which can be used to build different logic gates. At first, we designed an AND logic gate (Figure 4A). Cd^{2+} and DNA1 were utilized as the two inputs. The presence and absence of the inputs are set as 1 and 0, respectively. The output is the fluorescence value at 610 nm. The signal higher than the threshold value of 2×10^6 is defined as 1 (On state), while that lower than the threshold value is defined as 0 (Off state). Without any inputs (0,0) or with either input (1,0; 0,1) in the sensing system, no active Mg^{2+}-dependent DNAzyme could be formed and the G-rich sequence (domain 9) in H1

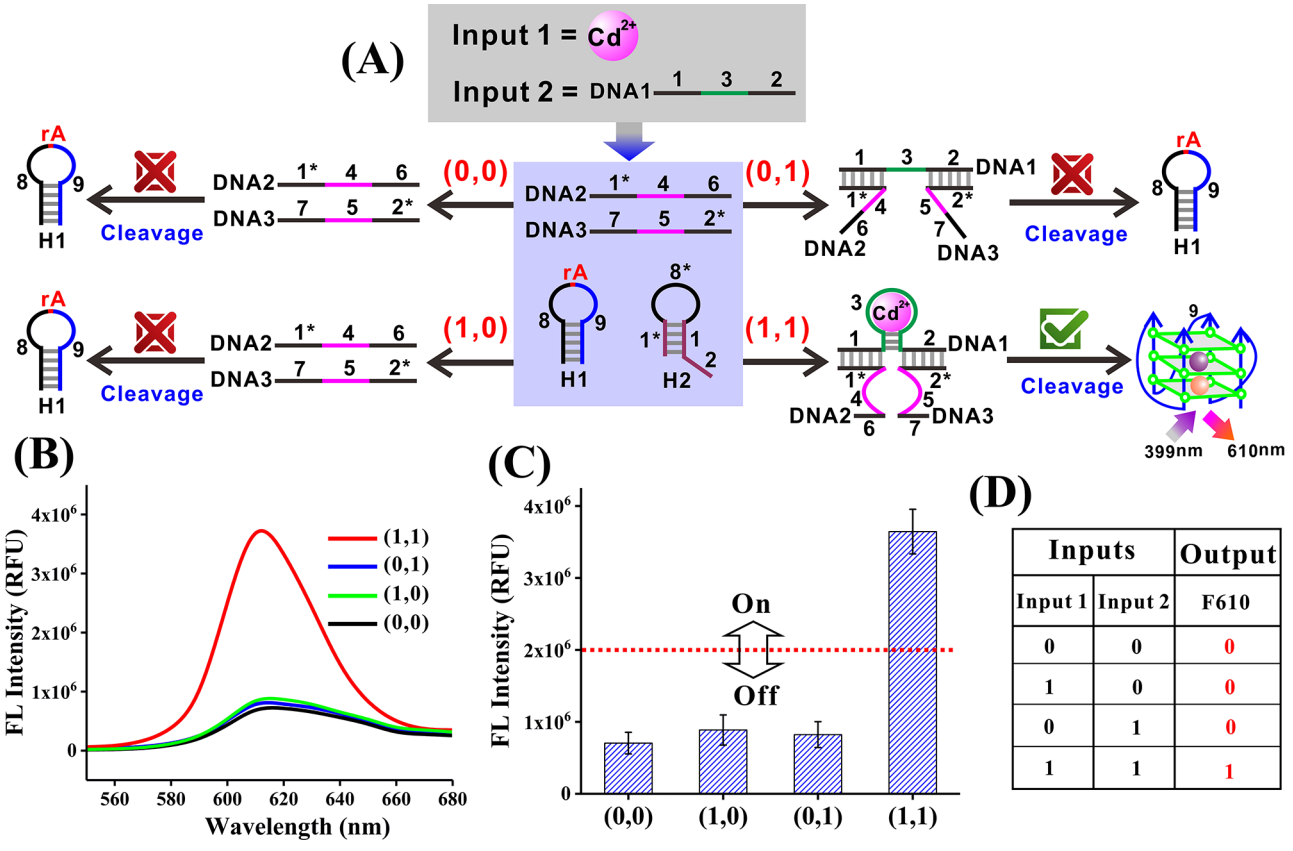

Figure 4. (A) Schematic representation of an AND logic gate. (B) The fluorescence spectra of the sensing platform depicting the AND gate. (C) The corresponding fluorescence values at 610 nm. The red dashed line is the threshold value of 2×10^6. (D) The truth table depicting the AND logic gate.

https://dx.doi.org/10.1021/acs.analchem.0c01022
Anal. Chem. 2020, 92, 6173−6180

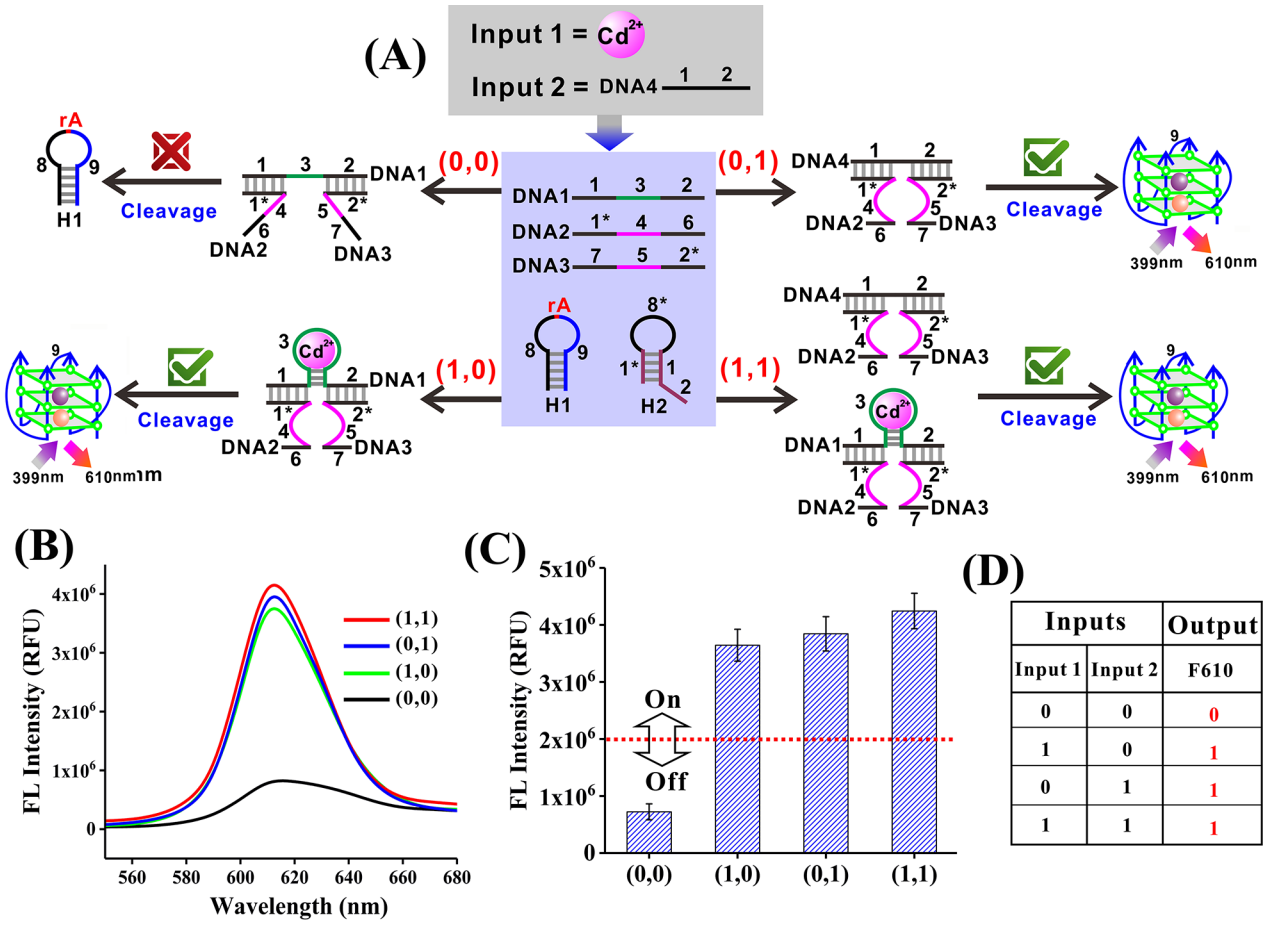

Figure 5. (A) Schematic representation of an OR logic gate. (B) The fluorescence spectra of the sensing platform depicting the OR gate. (C) The corresponding fluorescence values at 610 nm. The red dashed line is the threshold value of 2×10^6. (D) The truth table depicting the OR logic gate.

was still blocked. Only low fluorescence response (output = 0) was observed in such input combinations because no G-quadruplex DNAzyme was generated. In the presence of both inputs (1,1), an active DNAzyme can be formed though synergistic hybridization, and H1 will be cleaved into two fragments to produce a high fluorescence response (output = 1). The fluorescence spectra of the AND logic gate were shown in Figure 4B. The corresponding fluorescence intensities at 610 nm were shown in Figure 4C. A truth table was given in Figure 4D.

OR Logic Gate. An OR logic gate was fabricated using Cd^{2+} and DNA4 as the inputs. DNA4 (domains 1 and 2) is complementary to the recognition arms (domain 1* of DNA2 and domain 2* of DNA3) of the DNAzyme subunits. As shown in Figure 5A, in the absence of any inputs (0,0), DNA2 and DNA3 kept a long distance in the DNA1−DNA2−DNA3 complex, thus failing to generate an active DNAzyme and the repose signal was low (output = 0). In the presence of either (1,0; 0,1) or both inputs (1,1), the synergistically stabilized DNA structures (DNA1/Cd^{2+}−DNA2−DNA3 or DNA4−DNA2−DNA3) will be formed to produce active Mg^{2+}-dependent DNAzymes. The released domain 9 in H1 after the cleavage reaction will fold into the G-quadruplex DNAzyme structure, which can generate a high fluorescence signal (output = 1). The fluorescence spectra of the OR logic gate are shown in Figure 5B. The corresponding fluorescence intensities at 610 nm are shown in Figure 5C. A truth table was given in Figure 5D.

INHIBIT Logic Gate. In an INHIBIT logic gate design, we assigned the Cd^{2+}−DNA1 complex as the input 1 and DNA5 as the input 2. As illustrated in Figure 6A, in the absence of any inputs (0,0), no reaction happened (output = 0). In the presence of input 1 (1,0), an active DANzyme was formed, resulting in the cleavage of the substrate to give a high fluorescence value (output = 1). In the presence of another input (0,1), the system failed to yield any active DANzyme for readout because of the identical DNA sequences between the recognition arms (domains 1* and 2*) and the input 2. Thus, the platform produced a low fluorescence signal (output = 0). When both inputs (1,1) were present, a duplex structure (DNA1−DNA5) between input 1 and input 2 was formed. This prohibited the formation of an active DANzyme and the domain 9 in H1 was inaccessible. Only background signal was observed for this input combination (output = 0). The fluorescence spectra of the INHIBIT logic gate are shown in Figure 6B. The corresponding fluorescence intensities at 610 nm are shown in Figure 6C. A truth table is given in Figure 6D.

IMPLICATION Logic Gate. An IMPLICATION logic gate, which exhibited the reverse output results of an INHIBIT logic gate was also fabricated in the sensing platform. For the IMPLICATION logic gate design, Cd^{2+}−DNA6 complex and DNA 7 were employed as the two inputs. Meanwhile, DNA8 was introduced into the sensing system, which contained the

https://dx.doi.org/10.1021/acs.analchem.0c01022
Anal. Chem. 2020, 92, 6173−6180

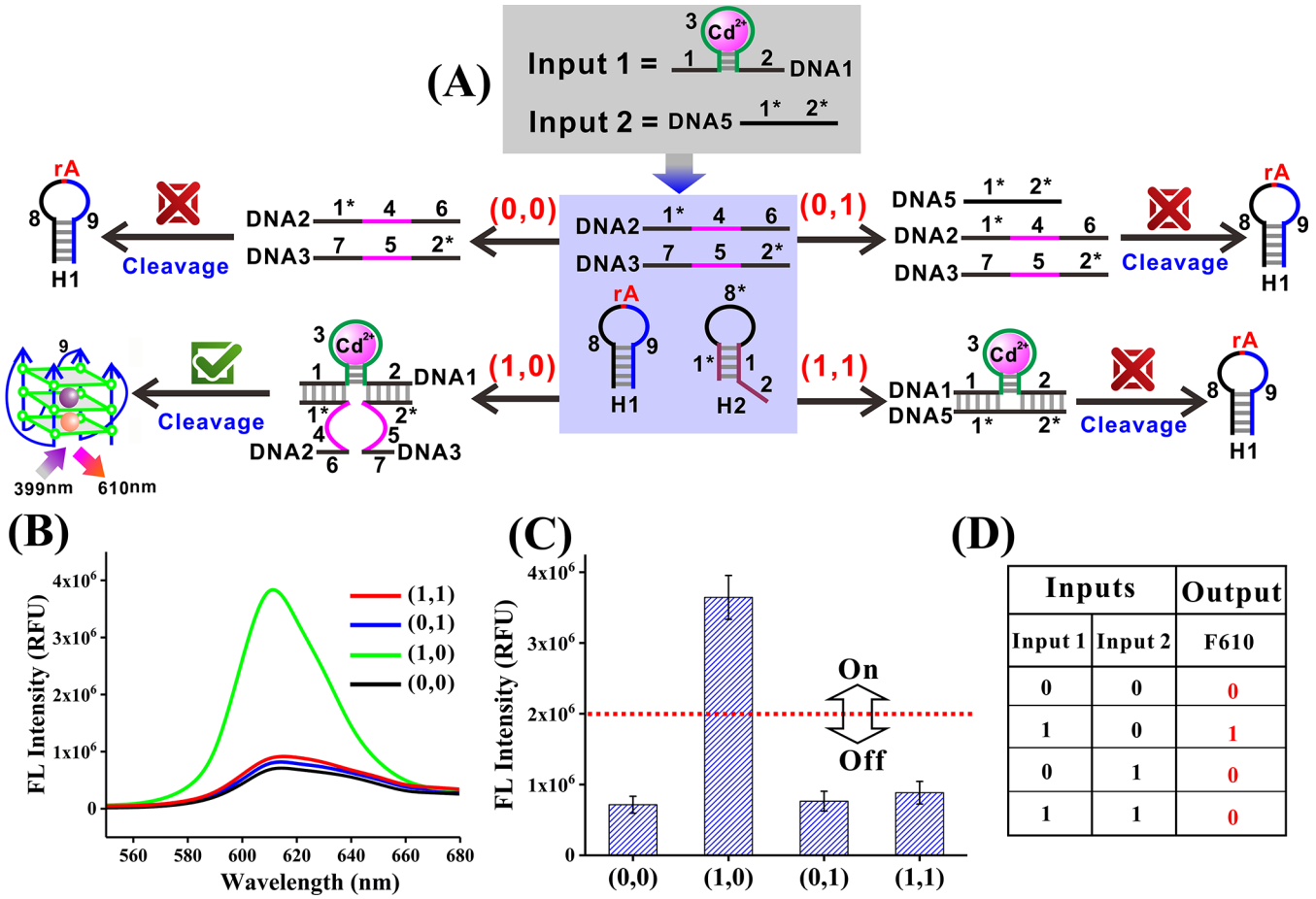

Figure 6. (A) Schematic representation of an INHIBIT logic gate. (B) The fluorescence spectra of the sensing platform depicting the INHIBIT gate. (C) The corresponding fluorescence values at 610 nm. The red dashed line is the threshold value of 2×10^6. (D) The truth table depicting the INHIBIT logic gate.

domains 1 and 2. As shown in Figure S7A (Supporting Information), in the absence of any inputs (0,0), DNA8 can hybridize with DNA2 and DNA3 to form an active DNAzyme (DNA8−DNA2−DNA3), giving rise to the output of 1. In the (1,0) input combination, domain a in DNA6 can be used as a toehold to start the toehold-mediated strand displacement reaction to displace the DNAzyme subunit (DNA2) from DNA8, triggering the disassembly of the active DNAzyme. As expected, the disassembly of the active DNAzyme resulted in a false result (ouput = 0). In the (0,1) and (1,1) combinations, the toehold-mediated strand displacement reactions were prohibited for the disassembly processes, because there was no toehold binding between the inputs and DNA8. Thus, the formed active DNAzyme kept the intact structure for the cleavage of the substrate and the output was 1. The fluorescence spectra of the IMPLICATION logic gate are shown in Figure S7B. The corresponding fluorescence intensities at 610 nm are shown in Figure S7C. A truth table is given in Figure S7D.

NOR Logic Gate. Using Cd^{2+}−DNA6 complex and DNA9 as the two inputs, we constructed a NOR logic gate. As illustrated in Figure S8A (Supporting Information), in the (0,0) state, DNA10 can hybridize with DNA2 and DNA3 to generate an active DNAzyme that will cleave H1 and the output is 1. In the (1,0) state, domain a (toehold) of DNA6 will bind to domain a* of DNA10 and start a toehold-mediated strand displacement reaction to displace DNA2. This will lead to the disassembly of an active DNAzyme and the output is 0. In the (0,1) state, domain b* (toehold) of DNA9 hybridizes with domain b of DNA10 and initiates the toehold-mediated strand displacement reaction to displace DNA3. This results in the inactivation of the DNAzyme and produces an output of 0. Similarly, in the presence of both inputs (1,1), DNA2 and DNA3 are all displaced from DNA10 though the toehold displacement mechanism. This process results in the dissociation of the active DNAzyme, consequently leading to an output of 0. The fluorescence spectra of the NOR logic gate ae shown in Figure S8B. The corresponding fluorescence intensities at 610 nm are shown in Figure S8C. A truth table is given in Figure S8D.

NAND Logic Gate. We further designed a NAND logic gate using Cd^{2+}−DNA6 complex and DNA9 as the two inputs. DNA11 in the sensing system contained duplicate regions of 1 and 2. As depicted in Figure S9A (Supporting Information), in the absence of any inputs (0,0), DNA11 bridged the DNA2 and DNA3 to assemble two active DNAzymes. This leads to the cleavage of H1 and the output is 1. In the presence of either input 1 (1,0) or input 2 (0,1), the input-initiated toehold-mediated strand-displacement reaction could disassemble one of the formed two active DNAzyme structures using segments a or b* as the toehold hybridization fragments. The other DNAzyme was still kept intact and active and led to the cleavage of H1 and also yielded a output of 1. When both inputs (1,1) were added, the hybridization of the inputs to

https://dx.doi.org/10.1021/acs.analchem.0c01022
Anal. Chem. 2020, 92, 6173−6180

DNA11 eliminated the two active DNAzymes, resulting in the output of 0. The fluorescence spectra of the NAND logic gate are shown in Figure S9B. The corresponding fluorescence intensities at 610 nm are shown in Figure S9C. A truth table is given in Figure S9D.

Logic Gate Application in Rice Samples. To demonstrate the robustness of the logic gate, we employed the OR logic gate to be operated in rice samples. Genetically modified (GM) rice with inserted exogenous genes often possesses improved characteristics, such as herbicide-tolerance and insect-resistance. However, there are public concerns about the food safety of the transgenic rice. Thus, it is important to detect the introduced gene in the rice sample to distinguish the GM events. GM rice may be contaminated with heavy metals at the same time. Thus, in the OR logic gate, Cd^{2+} (100 nM) and the specific gene (DNA4, 60 nM) were used as the two inputs at the same time. As shown in Figure S10 (Supporting Information), in the absence of the spiked Cd^{2+} and DNA4 (0,0), only very weak fluorescence signal appeared. When the rice sample were spiked with either Cd^{2+} (1,0), or DNA4 (1,0), or both inputs (1,1), a high fluorescence signal response can be observed. Thus, either or both inputs can generate a output of 1, giving rise to an OR gate computation in real agricultural products. The results indicated that our constructed logic system can perform the logic functions well even in complex sample matrixes.

CONCLUSION

In conclusion, we have designed a versatile sensing system for the label-free detection of Cd^{2+} based on DNAzyme-mediated cyclic signal amplification strategy and toehold stand displacement reaction. Anti-Cd^{2+} aptamer was employed as the binding sequence, and G-quadruplex was used as the reporting probe to construct the biosensor. Mg^{2+}-dependent DNAzyme was utilized to amplify the detection signal due to its multiple cleavage capability to the substrate. The sensing system is sensitive for Cd^{2+} detection, with a LOD of 2.5 pM. Also, the proposed assay exhibited outstanding specificity for Cd^{2+}. The developed sensing platform is robust and can be used to quantify the Cd^{2+} concentration in rice samples with good accuracy. Due to the unique advantages of label-free design, simple operation, and efficient signal amplification process, our proposed sensing protocol is particularly suitable for the routine monitoring of Cd^{2+} with high sensitivity and selectivity. More importantly, the flexible design of this sensing system enables us to construct some elegant logic gates, including AND, OR, INHIBIT, IMPLICATION, NOR, and NAND.

ASSOCIATED CONTENT

Supporting Information

The Supporting Information is available free of charge at https://pubs.acs.org/doi/10.1021/acs.analchem.0c01022.

Additional characterization data and spectra (PDF)

AUTHOR INFORMATION

Corresponding Author

Junhua Chen − *Guangdong Key Laboratory of Integrated Agro-environmental Pollution Control and Management, Guangdong Institute of Eco-environmental Science & Technology, Guangzhou 510650, China; National-Regional Joint Engineering Research Center for Soil Pollution Control and Remediation in South China, Guangzhou 510650, China;* orcid.org/0000-0001-9450-7272; Email: 222chenjunhua@163.com, jhchen@soil.gd.cn

Authors

Jiafeng Pan − *Guangdong Key Laboratory of Integrated Agro-environmental Pollution Control and Management, Guangdong Institute of Eco-environmental Science & Technology, Guangzhou 510650, China; National-Regional Joint Engineering Research Center for Soil Pollution Control and Remediation in South China, Guangzhou 510650, China*

Chengshuai Liu − *State Key Laboratory of Environmental Geochemistry, Institute of Geochemistry, Chinese Academy of Sciences, Guiyang 550081, China;* orcid.org/0000-0003-0133-0119

Complete contact information is available at: https://pubs.acs.org/10.1021/acs.analchem.0c01022

Notes

The authors declare no competing financial interest.

ACKNOWLEDGMENTS

This work was supported by the Guangdong Natural Science Funds for Distinguished Young Scholar (Grant 2016A030306012) and the Local Innovative and Research Teams Project of Guangdong Pearl River Talents Program (Grant 2017BT01Z176).

REFERENCES

(1) Yu, Y.; Zhou, X.; Zhu, Z.; Zhou, K. *J. Agric. Food Chem.* **2019**, *67*, 433−440.
(2) Chai, X.; Zhang, L.; Tian, Y. *Anal. Chem.* **2014**, *86*, 10668−10673.
(3) Zhou, D.; Wu, W.; Li, Q.; Pan, J.; Chen, J. *Anal. Methods* **2019**, *11*, 3546−3551.
(4) Rezvani, S. A.; Soleymanpour, A. *J. Chromatogr. A* **2016**, *1436*, 34−41.
(5) Yuan, X.; Yang, L.; Liu, S.; Yang, H.; Tang, Y.; Huang, K.; Zhang, M. *Anal. Methods* **2018**, *10*, 4821−4826.
(6) Londonio, A.; Morzan, E.; Smichowski, P. *Food Chem.* **2019**, *284*, 149−154.
(7) Duarte, K.; Justino, C. I. L.; Freitas, A. C.; Gomes, A. M. P.; Duarte, A. C.; Rocha-Santos, T. A. P. *TrAC, Trends Anal. Chem.* **2015**, *64*, 183−190.
(8) Zhou, W.; Saran, R.; Liu, J. *Chem. Rev.* **2017**, *117*, 8272−8325.
(9) Lopez Marzo, A.; Pons, J.; Blake, D. A.; Merkoci, A. *Anal. Chem.* **2013**, *85*, 3532−3538.
(10) Lopez-Marzo, A.; Pons, J.; Blake, D. A.; Merkoci, A. *Biosens. Bioelectron.* **2013**, *47*, 190−198.
(11) Guo, Y.; Zhang, Y.; Shao, H.; Wang, Z.; Wang, X.; Jiang, X. *Anal. Chem.* **2014**, *86*, 8530−8534.
(12) Xue, H.; Chen, Q.; Jiang, F.; Yuan, D.; Lv, G.; Liang, L.; Liu, L.; Hong, M. *Chem. Sci.* **2016**, *7*, 5983−5988.
(13) Knight, A. S.; Zhou, E. Y.; Francis, M. B. *Chem. Sci.* **2015**, *6*, 4042−4048.
(14) Zhang, Z.; Zhang, Z.; Liu, H.; Mao, X.; Liu, W.; Zhang, S.; Nie, Z.; Lu, X. *Biosens. Bioelectron.* **2018**, *103*, 87−93.
(15) Huang, P. J.; Liu, J. *Nucleic Acids Res.* **2015**, *43*, 6125−6133.
(16) Kasprowicz, A.; Stokowa-Soltys, K.; Wrzesinski, J.; Jezowska-Bojczuk, M.; Ciesiolka, J. *Dalton Trans.* **2015**, *44*, 8138−8149.
(17) Tang, W.; Wang, Z.; Yu, J.; Zhang, F.; He, P. *Anal. Chem.* **2018**, *90*, 8337−8344.
(18) Wang, X.; Gao, W.; Yan, W.; Li, P.; Zou, H.; Wei, Z.; Guan, W.; Ma, Y.; Wu, S.; Yu, Y.; Ding, K. *ACS Appl. Nano Mater.* **2018**, *1*, 2341−2346.
(19) Wang, H.; Cheng, H.; Wang, J.; Xu, L.; Chen, H.; Pei, R. *Talanta* **2016**, *154*, 498−503.

(20) Zeng, L.; Gong, J.; Rong, P.; Liu, C.; Chen, J. *Talanta* **2019**, *198*, 412−416.
(21) Li, F.; Zhang, H.; Wang, Z.; Newbigging, A. M.; Reid, M. S.; Li, X.; Le, X. C. *Anal. Chem.* **2015**, *87*, 274−292.
(22) Wu, Y.; Zhan, S.; Wang, L.; Zhou, P. *Analyst* **2014**, *139*, 1550−1561.
(23) Lotfi Zadeh Zhad, H. R.; Rodriguez Torres, Y. M.; Lai, R. Y. *J. Electroanal. Chem.* **2017**, *803*, 89−94.
(24) Zhu, Y.; Wang, Y.; Zhou, B.; Yu, J.; Peng, L.; Huang, Y.; Li, X.; Chen, S.; Tang, X.; Wang, X. *Anal. Bioanal. Chem.* **2017**, *409*, 4951−4958.
(25) Zhan, S.; Wu, Y.; Wang, L.; Zhan, X.; Zhou, P. *Biosens. Bioelectron.* **2016**, *86*, 353−368.
(26) Zhao, Y.; Chen, F.; Li, Q.; Wang, L.; Fan, C. *Chem. Rev.* **2015**, *115*, 12491−12545.
(27) Zeng, L.; Zhou, D.; Gong, J.; Liu, C.; Chen, J. *Anal. Chem.* **2019**, *91*, 1724−1727.
(28) Li, J.; Fu, W.; Wang, Z.; Dai, Z. *Chem. Sci.* **2019**, *10*, 5616−5623.
(29) Li, X.; Cui, Y.; Du, Y.; Tang, A.; Kong, D. *ACS Sens.* **2019**, *4*, 1090−1096.
(30) Li, Y.; Wang, G. A.; Mason, S. D.; Yang, X.; Yu, Z.; Tang, Y.; Li, F. *Chem. Sci.* **2018**, *9*, 6434−6439.
(31) Li, C.; Liu, W.; Hu, J.; Zhang, C. *Chem. Sci.* **2019**, *10*, 8675−8684.
(32) He, P.; Lou, X.; Woody, S. M.; He, L. *ACS Sens.* **2019**, *4*, 992−1000.
(33) Simmel, F. C.; Yurke, B.; Singh, H. R. *Chem. Rev.* **2019**, *119*, 6326−6369.
(34) Wang, H.; Wang, H.; Wu, Q.; Liang, M.; Liu, X.; Wang, F. *Chem. Sci.* **2019**, *10*, 9597−9604.
(35) Yang, L.; Wu, Q.; Chen, Y.; Liu, X.; Wang, F.; Zhou, X. *ACS Sens.* **2019**, *4*, 110−117.
(36) Liu, X.; Li, X.; Gao, X.; Ge, L.; Sun, X.; Li, F. *ACS Appl. Mater. Interfaces* **2019**, *11*, 15381−15388.
(37) Peng, H.; Newbigging, A. M.; Wang, Z.; Tao, J.; Deng, W.; Le, X. C.; Zhang, H. *Anal. Chem.* **2018**, *90*, 190−207.
(38) Lilienthal, S.; Klein, M.; Orbach, R.; Willner, I.; Remacle, F.; Levine, R. D. *Chem. Sci.* **2017**, *8*, 2161−2168.
(39) Tregubov, A. A.; Nikitin, P. I.; Nikitin, M. P. *Chem. Rev.* **2018**, *118*, 10294−10348.
(40) Ge, L.; Wang, W.; Sun, X.; Hou, T.; Li, F. *Anal. Chem.* **2016**, *88*, 9691−9698.
(41) Deng, J.; Tao, Z.; Liu, Y.; Lin, X.; Qian, P.; Lyu, Y.; Li, Y.; Fu, K.; Wang, S. *Chem. Commun.* **2018**, *54*, 3110−3113.
(42) Guo, Y.; Zhang, Y.; Shao, H.; Wang, Z.; Wang, X.; Jiang, X. *Anal. Chem.* **2014**, *86*, 8530−8534.
(43) Abbasi Tarighat, M.; Mohammadizadeh, M. R.; Abdi, G. *J. Agric. Food Chem.* **2013**, *61*, 6832−6840.
(44) Zhao, J.; Zhang, L.; Jiang, J.; Shen, G.; Yu, R. *Chem. Commun.* **2012**, *48*, 4468−4470.
(45) Pan, J.; Zeng, L.; Chen, J. *Chem. Commun.* **2019**, *55*, 11932−11935.

https://dx.doi.org/10.1021/acs.analchem.0c01022
Anal. Chem. 2020, 92, 6173−6180